Free-energy model for fluid helium at high density

Christophe Winisdoerffer, Gilles Chabrier

Free-energy model for fluid helium at high density

Christophe Winisdoerffer[1,2,*] and Gilles Chabrier[2,†]
[1]*Theoretical Astrophysics Group, University of Leicester, Leicester, LE1 7RH, United Kingdom*
[2]*École Normale Supérieure de Lyon, CRAL (UMR CNRS No. 5574), 69364 Lyon Cedex 07, France*
(Received 15 October 2004; published 7 February 2005)

We present a semianalytical free-energy model aimed at characterizing the thermodynamic properties of dense fluid helium, from the low-density atomic phase to the high-density fully ionized regime. The model is based on a free-energy minimization method and includes various different contributions representative of the correlations between atomic and ionic species and electrons. This model allows the computation of the thermodynamic properties of dense helium over an extended range of density and temperature and leads to the computation of the phase diagram of dense fluid helium, with its various temperature and pressure ionization contours. One of the predictions of the model is that pressure ionization occurs abruptly at $\rho \gtrsim 10$ g cm^{-3}, i.e., $P \gtrsim 20$ Mbar, from atomic helium He to fully ionized helium He^{2+}, or at least to a strongly ionized state, without a He^{+} stage, except at high enough temperature for temperature ionization to become dominant. These predictions and this phase diagram provide a guide for future dynamical experiments or numerical first-principle calculations aimed at studying the properties of helium at very high density, in particular its metallization. Indeed, the characterization of the helium phase diagram bears important consequences for the thermodynamic, magnetic, and transport properties of cool and dense astrophysical objects, among which are the solar and the numerous recently discovered extrasolar giant planets.

DOI: 10.1103/PhysRevE.71.026402 PACS number(s): 52.25.Jm, 05.70.Ce, 52.25.Kn, 64.30.+t

I. INTRODUCTION

Within the past decade, over a hundred brown dwarfs, astrophysical bodies not dense enough to sustain hydrogen fusion in their core, and extrasolar giant planets, i.e., jovian planets orbiting stars outside the solar system, have been discovered. These objects are composed essentially of hydrogen and helium. Given their large gravity and relatively low temperature, within astrophysical standards, the hydrogen and heluim fluid is in an atomic or molecular form in the outermost part of the body and in the form of a fully ionized electron-ion plasma in the innermost regions. Such an internal structure is common to many so-called compact objects, from our own jovian planets to the external layers of white dwarfs or neutron stars. The characterization of the structure and cooling properties of these compact objects thus requires the knowledge of the thermodynamic properties of dense hydrogen and helium fluids, and more importantly a realistic description of the partial, pressure ionization regime. Given the large variations of thermodynamic conditions characteristic of the structure and evolution of such astrophysical bodies, these thermodynamic properties, characterized by the equation of state (EOS), must be calculated over several orders of magnitudes in density and temperature. As discussed below, the necessity to calculate the thermodynamic properties over such a large range of conditions precludes the use of heavy computer simulations and thus necessitates the derivation of EOS models which allow extensive calculations within a reasonable amount of computer time, unfortunately at the price of a more approximate, or say phenomenological description of the properties of matter at high density.

Interestingly enough, these EOS's of dense matter under astrophysical conditions can now be probed on Earth by shock-wave experiments. Future large laser experiments, like, e.g., the NIF project at Livermore or the LMJ project in France, will reach conditions characteristic of the deep interior of the aforementioned astrophysical bodies. So not only is the calculation of dense matter EOS of interest for astrophysical applications, but it is necessary for the confrontation of theory with existing and future high-pressure experiments, yielding eventually a correct knowledge of the properties of matter under extreme conditions. Hydrogen, the most common element in the universe, has been studied extensively, on both the experimental and theoretical fronts, and the EOS of dense hydrogen becomes more and more constrained, although the very regime of pressure ionization still remains ill determined. The same cannot be said for helium. Although some experiments exist in the regime of neutral helium at high density, as detailed below, the regime of helium pressure ionization, from He to He^{+} and He^{2+} remains for now unexplored, and no attempt has been made to give a detailed theoretical description of these domains. It is the very purpose of the present paper to derive an EOS for dense, partially ionized helium, covering the gap between the previous study of dense neutral helium [1] and the fully ionized regime [2,3]. As mentioned above, not only is the calculation of such a dense helium EOS necessary for a description of the thermodynamic properties of astrophysical compact objects, in particular the recently discovered gaseous exoplanets, but it provides a useful guide for future high-pressure shock-wave or laser experiments.

The paper is organized as follows. In Sec. II, we briefly comment on the general formalism underlying the present calculations. The various contributions entering our general model free energy are presented in detail in Sec. III. The

*Electronic address: cwinisdo@ens-lyon.fr
†Electronic address: chabrier@ens-lyon.fr

results and the limitations of the model are presented in Sec. IV. Special attention is devoted to the impact of various approximations in the free-energy calculation on the final results. Section V is devoted to the conclusion.

II. GENERAL CONSIDERATIONS

A. Chemical picture of a dense plasma

Equation-of-state calculations can be divided into two generic categories. The "physical approach" is formally exact as it involves only fundamental particles, electrons and nuclei, interacting through the Coulomb potential. The partition function is calculated using the eigenvalues corresponding to this N-body system. In practice, however, the exact solution cannot be calculated, in particular when bound states form, and either perturbative expansions or approximate numerical schemes must be used. The validity of the expansions is limited to high temperatures and/or low densities, i.e., apply to weakly or moderately coupled plasmas. The regime of pressure ionization thus cannot be described by such expansion schemes. Numerical techniques, such as density functional theory, molecular dynamics, or path-integral Monte Carlo simulations, do extend to the strongly correlated regime but the description of the pressure ionization regime then becomes a formidable task, and involves also physical approximations in the calculations of either the electron functional or the nodal functions, not mentioning the finite size effects due to the limited number of particles in the simulation. In practice, these simulations do not allow the calculation of thermodynamic quantities over a large range of temperatures and densities, as needed for practical applications, as mentioned earlier. For this reason, a more phenomenological approach has been developed which combines a simplified description of the properties of dense matter and a semianalytical derivation, allowing the calculations of extended thermodynamic tables with moderate computer time investment. This is the so-called "chemical picture." In this approach, the basic particles are no longer only electrons and nuclei but also bound species (atoms, molecules, ions), which are characterized by their interparticle potentials. That means that the particles remain distinguishable (in a classical sense) in the plasma, with their own identities and interaction properties. The problem thus reduces to the free-energy minimization of a multicomponent system, taking into account chemical and ionization equilibrium between the various species. Although certainly of doubtful validity in the regime of pressure ionization, where the concepts of pair potential and bound states become meaningless, this approach has been shown to yield reasonably accurate descriptions of hydrogen at high density [4,5]. Moreover, as mentioned above, this approach presents the advantage of being semianalytical and thus has a valuable practical interest for EOS calculations. Last but not least, the chemical approach offers the noticeable advantage of clearly identifying the terms and the approximations aimed at describing various physical effects. Such terms can be added or removed with limited effort, allowing a rapid identification of the dominant contributions responsible for the thermodynamic properties of matter under complex conditions. Therefore, despite its shortcomings, the chemical approach should be seen as a useful alternative to the "exact" physical approach.

B. General free-energy model

The chemical approach is based on the minimization of the free energy $F(\{N_i\},T,V)$ corresponding to a system containing $\{N_i\}$ different species inside a volume V at temperature T. This minimization $\delta F=\Sigma_i(\partial F/\partial N_i)\delta N_i=0$ must satisfy the electroneutrality condition and the stoichiometric conditions corresponding in our case to the following set of chemical equations:

$$\mathrm{He} \leftrightharpoons \mathrm{He}^+ + e^-,$$

$$\mathrm{He}^+ \leftrightharpoons \mathrm{He}^{2+} + e^-. \tag{1}$$

The canonical partition function of the system $\mathcal{Z}$ is assumed to be factorizable into different contributions, so that the free energy $F=-kT\ln\mathcal{Z}$ can be split into the sum of translational, configurational, and internal contributions [6,7]. Adding up the correction arising from the quantum behavior of the heavy particles, one gets

$$F(\{N_i\},T,V) = F_{\mathrm{id}}(\{N_i\},T,V) + F_{\mathrm{conf}}(\{N_i\},T,V) + F_{\mathrm{int}}(\{N_i\},T,V) + F_{\mathrm{qm}}(\{N_i\},T,V). \tag{2}$$

The conditions of validity of such a separability are as follows.

(1) The discretization of the eigenvalues corresponding to the translational degrees of freedom and to the center-of-mass positions is negligible. This is the quasiclassical approximation.

(2) There is no coupling between the translation degrees of freedom and the center-of-mass positions.

(3) The internal energy levels remain essentially unperturbed by the interactions with surrounding particles.

If the two first conditions are satisfied in the present context, the last one certainly becomes invalid in the pressure ionization regime. We expect this regime, however, to cover a limited range of density, as pressure ionization generally occurs rather abruptly. Eventually, only comparison with experimental data can give a quantitative estimate of the discrepancy due to this underlying factorization condition. The various contributions to F are described in the next section.

III. FREE-ENERGY MODEL

We first present the models used to calculate the contributions to the total free energy arising from each different species He, He^+, and He^{2+}. Then, we describe the modelization of the coupling between these various species.

A. Model for atomic helium He

1. The kinetic free energy F_{id}

The ideal part of the free energy, corresponding to the kinetic part of the Hamiltonian, is given by [8]

$$F_{\mathrm{id}}(N,T,V) = -Nk_BT\left\{1+\ln\left[\frac{V}{N}\left(\frac{2\pi Mk_BT}{h^2}\right)^{3/2}\right]\right\}, \quad (3)$$

where N is the number of helium atoms of mass M inside the volume V at temperature T.

2. The configurational free energy F_{conf}

The configurational free energy F_{conf}, arising from the interactions between helium atoms, is calculated within the Weeks-Chandler-Andersen (WCA) perturbation theory [9,10]. The interaction potential $\Phi(r)$ is split into a reference potential $\Phi_{\mathrm{ref}}(r)$ and a perturbative part $\Phi_{\mathrm{pert}}(r)$. Truncating the perturbative expansion of the free energy after the first order, the so-called high-temperature approximation (HTA) yields

$$F_{\mathrm{conf}} = F_{\mathrm{ref}}(T,V,N) + \frac{N^2}{2V}\int d\boldsymbol{r}\Phi_{\mathrm{pert}}(r)g_{\mathrm{ref}}(r,V,N). \quad (4)$$

The problem is thus reduced to the potential separation and to the calculation of $F_{\mathrm{ref}}(T,V,N)$ and $g_{\mathrm{ref}}(r,V,N)$. Concerning the first point, we use a modification of the procedure of Kang *et al.* [11], namely,

$$\Phi_{\mathrm{ref}}(r) = \begin{cases} \Phi(r) - \left(\Phi(\lambda) + \left.\dfrac{d\Phi}{dr}\right|_{r=\lambda}(r-\lambda)\right) & \text{if } r<\lambda, \\ 0 & \text{if } r\geqslant\lambda, \end{cases} \quad (5)$$

$$\Phi_{\mathrm{pert}}(r) = \begin{cases} \Phi(\lambda) + \left.\dfrac{d\Phi}{dr}\right|_{r=\lambda}(r-\lambda) & \text{if } r<\lambda, \\ \Phi(r) & \text{if } r\geqslant\lambda, \end{cases}$$

where $\lambda=(a_{\mathrm{fcc}}^{-3}+r^{*-3})^{-1/3}$; $a_{\mathrm{fcc}}=[\sqrt{2}/(N/V)]^{1/3}$ and r^* corresponds to the minimum of the potential $\Phi(r)$. This choice for the density-dependent break point λ has the advantage to give a continuously differentiable λ. Concerning the second point, we approximate the repulsive reference potential by a hard-sphere potential. The hard-sphere radius σ is calculated from the Barker-Henderson criterion:

$$\sigma_{\mathrm{BH}} = \int_0^\infty dr(1-e^{-\beta\Phi_{\mathrm{ref}}}) = \int_0^{\sigma_{\mathrm{BH}}} dr(1-e^{-\beta\Phi_{\mathrm{ref}}}), \quad (6)$$

with the Verlet and Weiss correction [12] to include a density dependence

$$\sigma = \sigma_{\mathrm{BH}}\left(1+\frac{\sigma_1}{2\sigma_0}\delta\right), \quad (7)$$

where δ is a function of the temperature and $\sigma_1/2\sigma_0$ is a function of T and σ. This nonlinear equation is solved by direct iteration, using σ_{BH} as an initial guess for $\sigma \equiv \sigma(T,n)$. An example of the evolution of σ with density and temperature is presented in Fig. 1. The free energy and the radial distribution functions for the hard-sphere reference system $F_{\mathrm{ref}}\equiv F_{\mathrm{HS}}$, $g_{\mathrm{ref}}\equiv g_{\mathrm{HS}}$, are obtained analytically [13,14].

To describe the interaction between two helium atoms, we choose the Aziz and Slaman [15] potential for $r\geqslant 1.8$ Å, and the Ceperley and Partridge [16] one for $r<1.8$ Å. Following Aparicio and Chabrier [1], this two-body potential is modified by a density-dependent function to mimic the softening due to N-body effects at high density:

$$\Phi(r) = \left((1-C)+\frac{C}{1+D\rho}\right)\Phi_{\rho\to 0}(r). \quad (8)$$

The two parameters C and D are optimized to reproduce the experimental measures of adiabatic sound velocity [17]. A χ^2 minimization yields $(C,D)=(0.44, 0.8\ \mathrm{cm}^3/\mathrm{g})$. This potential is illustrated in Fig. 2 whereas Fig. 3 compares the measured sound velocity and the one calculated with our potential. Figure 4 compares the Hugoniot curves obtained with the present atomic helium free-energy model and interatomic potential with presently available shock-wave experiments [18]. These comparisons assess the validity of the present model at least up to the limit of the data, i.e., $P\simeq 1$ Mbar.

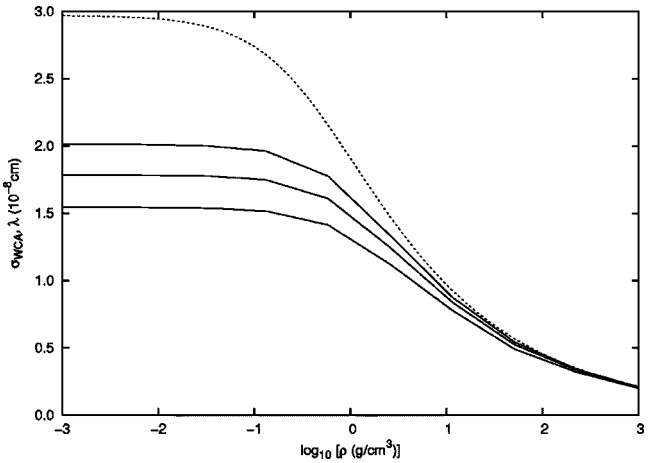

FIG. 1. Hard-sphere radii σ_{WCA} for atomic helium (solid line), for $T=10^{3.0}$, $10^{3.5}$, and $10^{4.0}$ K from top to bottom, and break point λ (dotted line) as a function of the density.

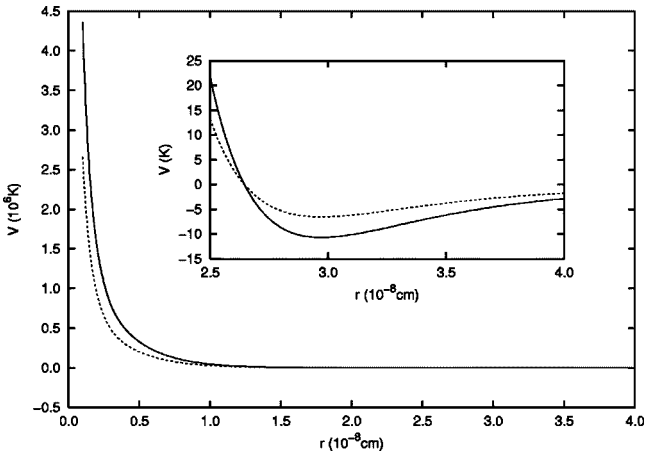

FIG. 2. Interaction potential between two helium atoms, without N-body correction (solid line) and with the N-body softening correction at $\rho=10\ \mathrm{g/cm}^3$ (dotted line).

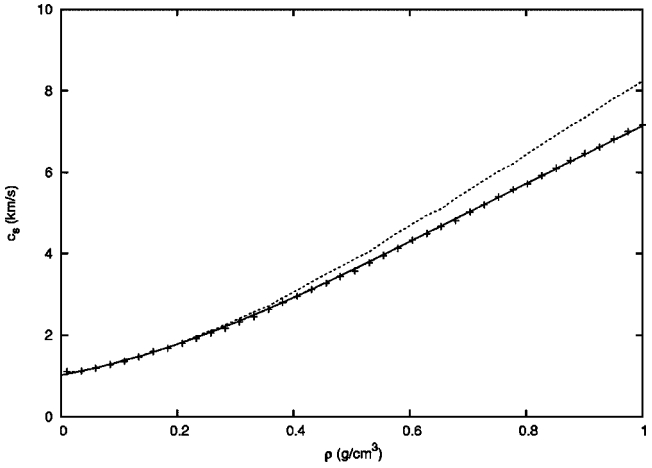

FIG. 3. Comparison between the experimental measures of the adiabatic sound velocity [17] (solid line) and the present calculations with $(C,D)=(0.44,0.8\ \mathrm{cm}^3/\mathrm{g})$ (crosses) and $(C,D)=(0,0\ \mathrm{cm}^3/\mathrm{g})$ (dotted line).

3. The internal free energy F_{int}

The divergence of the internal partition function $\Sigma_l g_l \exp(-E_l/k_BT)$ of an isolated atom is a well-known problem in statistical physics. It emphasizes the necessity to take into account the interactions between atoms in the calculation of the internal partition function $\mathcal{Z}_{\mathrm{int}}=\exp(-\beta F_{\mathrm{int}})$. For a density n, each atom has a typical available volume $n^{-1/3}$ so that, as density increases, the levels associated with the highest eigenvalues will move into the continuum. When the density is high enough to disturb even the ground state, the electrons can no longer remain bound to the nuclei: this is the pressure ionization phenomenon. We have included the effect of the interactions of surrounding particles on the internal partition function of helium within the so-called occupation probability formalism (OPF) [19]. The OPF ensures the statistical-mechanical consistency between the configurational free energy characterizing the interactions between atoms, F_{conf}, and the internal free-energy contribution, F_{int}. The OPF has been extensively presented in various papers (see, e.g., [20]), and is only briefly outlined for completeness. We consider a system of interacting particles, of free energy $F=F_{\mathrm{id}}-k_BT\ln\mathcal{Z}_{\mathrm{int}}+f$, where f is the nonideal term. Within the OPF, the total free energy can be rewritten under the form

$$F = F_{\mathrm{id}} - k_BT\ln\tilde{\mathcal{Z}} + f - \sum_\alpha N_\alpha \frac{\partial f}{\partial N_\alpha}, \tag{9}$$

with

$$\tilde{\mathcal{Z}} = \sum_\alpha \omega_\alpha g_\alpha e^{-\beta E_\alpha} \quad \text{and} \quad \omega_\alpha = \exp\left(-\beta\frac{\partial f}{\partial N_\alpha}\right). \tag{10}$$

The term ω_α can be seen as the probability that the eigenstate α of the atom still exists in the midst of the surrounding particles. These factors ω_α are calculated consistently from the configurational term f, and the term $\Sigma_\alpha N_\alpha \partial f/\partial N_\alpha$ ensures the statistical-mechanical consistency (see [19]). The OPF has several noticeable advantages, among which are the following.

(1) ω_α decreases monotonically and continuously with increasing density, ensuring the convergence of $\tilde{\mathcal{Z}}_{\mathrm{int}}$ and the derivability of F_{int}.

(2) No ill-controlled energy shifts of the levels are introduced, as required from the condition of factorizability of the partition function [Eq. (2)]. Experiments at low density [21] and calculations [22,23] do not show such energy shifts.

(3) The probabilistic interpretation of ω_α enables us to combine several occupation probabilities arising from statistically independent interactions. We will come back to this point in Sec. III D.

The exact solution, in principle, requires the knowledge of all the interaction potentials between an atom in state α and another one in state α'. In the absence of such information, we have adopted the simplest approach which consists of characterizing excited state interactions by hard-sphere excluded volumes in the phase space. The hard-sphere radii are calculated with the scaling law derived by Aparicio and Chabrier [1] [Eqs. (14a) and (14b)]. Within the first order in the expansion of the nonideal part f of the free energy [Eq. (4)], the $\omega_\alpha^{\mathrm{HS}}$ for the excited states are thus given by

$$\omega_\alpha^{\mathrm{HS}} = \exp\left(-\beta\frac{\partial f_{\mathrm{HS}}(\{N_\alpha\},V,T)}{\partial N_\alpha}\right). \tag{11}$$

This nonlinear equation is solved iteratively by using results obtained within the low excitation approximation (LEA) and low-density approximation (LDA), $\omega_\alpha^{\mathrm{HS,LEA+LDA}}=\exp[-\pi N(\sigma_\alpha+\sigma_1)^3/6V]$, as initial guess.

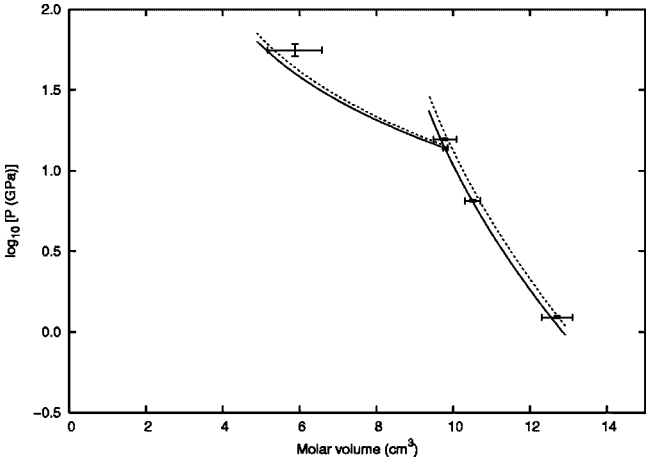

FIG. 4. Comparison between the experimental single- and double-shock Hugoniot curves [18] and the present calculations with $(C,D)=(0.44,0.8\ \mathrm{cm}^3/\mathrm{g})$ (solid line) and $(C,D)=(0,0\ \mathrm{cm}^3/\mathrm{g})$ (dotted line).

4. The quantum correction of the free energy F_{qm}

We have taken into account the correction to the free energy arising from quantum effects due to the finite size of the atoms by keeping the first order of the Wigner-Kirkwood $\hbar^2$ expansion of $\mathrm{Tr}[e^{-\beta H}]$ [24,25,8]:

$$F_{\rm qm} = \frac{\hbar^2}{24 k_B T V M_{\rm He}} N^2 \int d\boldsymbol{r}\, \boldsymbol{\nabla}^2 \Phi(r) g(r). \qquad (12)$$

$\Phi(r)$ corresponds to the potential shown in Sec. III A 2, and $g(r) \equiv y(r) e^{-\beta\Phi(r)}$ is approximated by $y_{\rm HS}(r) e^{-\beta\Phi(r)}$.

B. Model for the partially ionized plasma $\{He^+, e^-\}$

Because of the presence of bound states, the treatment of He^+ presents the same difficulties as for He. We adopt the same formalism, namely, the WCA perturbation expansion, to calculate the He^+ configurational free energy (with the hard-sphere model as the reference system) and the OPF to treat the internal partition function. For the long-range interaction potential between He^+ ions, we take a Yukawa potential $e^{-k_s r}/r$, where the density- and temperature-dependent screening wave vector is given by [26]

$$k_s(n,T) = \frac{1}{\sqrt{2}} k_{\rm TF} [\theta^{1/2} F_{-1/2}(\mu/k_B T)]^{1/2}, \qquad (13)$$

where $k_{\rm TF} = (4 m_e e^2/\pi\hbar^2)^{1/2} (3\pi^2 n_e)^{1/6}$ is the Thomas-Fermi screening wave vector, n_e is the total free electron density, $\theta = T/T_F$ is the electronic degeneracy parameter (T_F is the electron Fermi temperature), F_n is the Fermi integral of order n, and $\mu/k_B T$ is the electron chemical potential defined by $F_{1/2}(\mu/k_B T) = 2\theta^{-3/2}/3$.

For the treatment of the internal free energy, we need a scaling law to associate a hard-sphere radius with the excited states of He^+. Since He^+ is hydrogenlike, and the energy levels are degenerate toward the orbital quantum number l, we write this scaling law as

$$\sigma_n = n^2 \sigma_1, \qquad (14)$$

where σ_1 is the WCA hard-sphere radius associated with the ground state, and n is the main quantum number.

The calculations then proceed exactly as in Sec. III A.

C. Model for the fully ionized plasma $\{He^{2+}, e^-\}$

The free energy of a fully ionized electron-ion plasma (FIP) has been calculated by Chabrier and Potekhin [2] and Potekhin and Chabrier [3]. These authors provide analytical parametrizations for the various thermodynamic quantities. We refer the reader to these papers for a description of the fully ionized plasma model.

D. Interactions between different species

Besides all the afore-described contributions to the free energy, arising from interactions between species of same nature, we must also include contributions arising from the interactions between species of *different* nature.

1. Hard-sphere interactions between atoms and ions

The first-order interaction between the atomic and ionic species He, He^+, and He^{2+} is the hard-sphere excluded volume interaction, $F_{\rm HS}(\{N_{{\rm He},\alpha}, N_{{\rm He}^+,\alpha}, N_{{\rm He}^{2+}}\}, \{\sigma_{{\rm He},\alpha}, \sigma_{{\rm He}^+,\alpha}, \sigma_{{\rm He}^{2+}}\}, V, T)$, with a radius $\sigma_{{\rm He}^{2+}} \equiv 0$ for the He^{2+} ions, calculated consistently from the hard-sphere free energy of a multicomponent interacting system [13]. It can be shown easily that the contribution arising from the $\sigma_{{\rm He}^{2+}} = 0$ component is equivalent to renormalizing the ideal (kinetic) term for this species with a volume $V' = (1-\eta)V$, where $\eta = \Sigma_{i\in\{\rm HS\}} \pi n_i \sigma_i^3/6$ corresponds to the total packing fraction [4]. This term thus takes into account the He-He, He^+-He^+, He-He^+, He-He^{2+}, and He^+-He^{2+} interactions. Note that, in contrast to previous approaches, we do not consider excluded volume interactions between bound species and free electrons. Indeed, such an approach does not seem to be justified, for the quantum exclusion principle applies only to electrons in the same state. The entire volume of the system is thus available to the majority of the free electrons, even in the presence of bound species, as long as the free electrons are in a quantum state different from those corresponding to the bound states. In any event, we have checked that the introduction of an excluded volume for the electrons does not modify significantly the final results.

2. Induced interactions between atoms and ions

The presence of charges in the neighborhood of species with bound states has two consequences. The first one is the induced polarization due to the electronic cloud, which translates into a related contribution to the free energy. The second one is the induced Stark effect on the bound states, due to the ambient electric field which modifies the one associated with the atom nucleus. These two effects have been taken into account in our model as described below.

a. Polarization effects. The polarization contribution to the free energy arising from the interactions between the charges and the neutral atoms He has been handled as in previous N-body approaches [27,4]:

$$F_{\rm pol} = \frac{2 k_B T}{V} N_{\rm He} \sum_{i={\rm He}^+, {\rm He}^{2+}, e^-} N_i B_{{\rm He},i}. \qquad (15)$$

The second virial coefficients $B_{{\rm He},i}$ are given by

$$B_{{\rm He},i} = 2\pi \int_{\sigma_{{\rm He}\text{-}i}}^{\infty} dr\, r^2 (1 - e^{-\beta\Phi^i_{\rm pol}}), \qquad (16)$$

where

$$\Phi^i_{\rm pol}(r) = -\frac{Z_i e^2 \alpha_i}{2} \left[\frac{1 + k_s r}{r^2 + \sigma^2_{{\rm He}\text{-}i}}\right]^2 \exp(-2 k_s r) \qquad (17)$$

is the polarization potential between He and the species i. The two free parameters $\sigma_{{\rm He}\text{-}i}$ and α_i are the hard-core radius and the polarizability. For the He-He^{2+} and He-e^- interactions, the hard-core radius is chosen to be the He atom ground-state radius $\sigma^{\rm HS}_{\rm He\text{-}He}$, and the polarizability (which has the dimension of a volume) is equal to $(\sigma^{\rm HS}_{\rm He\text{-}He})^3$. For the He-$He^+$ interaction, the hard core radius is $\sigma^{\rm HS}_{{\rm He}\text{-}{\rm He}^+} = (\sigma^{\rm HS}_{\rm He\text{-}He} + \sigma^{\rm HS}_{{\rm He}^+\text{-}{\rm He}^+})/2$ and the polarizability is equal to $(\sigma^{\rm HS}_{{\rm He}\text{-}{\rm He}^+})^3$.

b. Electric microfield effects. The Stark effect on the bound states, arising from the electric microfield **E** due to the surrounding charges, is also treated within the framework of the OPF. The occupation probability associated with the Stark interaction on the internal states of He and He^+ is given by [19]

$$\omega_\alpha^{\mu E} = \int_0^{\beta_\alpha^{\rm crit}} d\beta\, \mathcal{P}(\beta), \tag{18}$$

where $\beta=(4\pi\varepsilon_0 a^2/Ze)E$ is the dimensionless electric field [Ze is the ion charge and $a=(4\pi n/3)^{-1/3}$ is the mean interparticle distance], $\mathcal{P}(\beta)$ is the probability that the central ionic center experiences a field between β and $\beta+d\beta$, and $\beta_\alpha^{\rm crit}$ is a critical field associated with each bound state α. Potekhin *et al.* [28] have calculated the microfield distribution of an atom (neutral ionic center) or an ion (charged ionic center) immersed in a surrounding ionized plasma. These calculations take into account the interactions in the plasma [$\Gamma=(Ze)^2/akT\neq 0$], and recover the Holtzmark limit in the case of a noninteracting, perfect gas ($\Gamma=0$). These authors provide analytical formulas for $Q(\beta,\Gamma)=\int_0^\beta dt\, \mathcal{P}(t,\Gamma)$ in the case of a neutral or a charged central ionic center. Note that $Q(\beta,\Gamma)$ and thus the probability $\omega_\alpha^{\mu E}$ depend not only on the temperature, as in the Holtzmark limit, but also on the density, through the parameter Γ. The critical fields are given by Hummer and Mihalas [19] in the case of a hydrogenlike system. We have directly applied their prescription to He^+, and used the similarity between a He atom and a hydrogenlike system, with a central charge equal to $7/4$ for the ground state and 1 for the $1snl$-type levels [1], to calculate the critical fields corresponding to atomic helium He.

3. Long-range interaction between He^+ and He^{2+}

The remaining coupling contribution between the various species stems from the long-range Coulomb interaction between helium ions He^+, He^{2+} and electrons. Short-distance interactions due to the internal levels of He^+ have been considered in the previous sections. The treatment of the long-range Coulomb interaction between the two ionic species will certainly have some impact in the pressure ionization regime where He^+ and He^{2+} coexist, but will not modify the rest of the phase diagram. This contribution, however, is difficult to evaluate accurately. Considering the He^+-He^{2+} interaction as a pure Coulomb contribution, thus representing the He^+-He^{2+} fluid as an interacting two-component $Z_1=1$, $Z_2=2$ point-charge plasma, is not satisfactory, for it precludes a correct treatment of the internal levels of He^+, which has been included in our formalism (see previous section). In this context, and in the absence of an accurate formulation, we estimate the contribution to the total free energy arising from the He^+, He^{2+}, e^- long-range interaction in the framework of the ion-sphere model [29], thus considering only the electrostatic contribution to the free energy. In this very simplified model, the interaction between He^+ and He^{2+} gives a contribution equal to $Z_1Z_2e^2/a$ per pair, with $Z_1=1$ and $Z_2=2$, whereas the contribution due to the interaction between the central ion He^+ and the uniformly charged sphere $-Z_1e$ gives a contribution $-3/2(Z_1e)^2/a$ per He^+. The He^{2+}-e^- and e^--e^- contributions are already included in the FIP model mentioned in Sec. III C. The contribution thus reads

$$F(N_{\rm He^+},N_{\rm He^{2+}}) = \frac{N_{\rm He^+}N_{\rm He^{2+}}}{2} Z_1Z_2\frac{e^2}{a} - \frac{3}{2}N_{\rm He^+}\frac{(Z_1e)^2}{a}. \tag{19}$$

The very crude treatment of this interaction between He^+, He^{2+} and electrons is certainly a major shortcoming of the present model and Eq. (19) gives at best the order of magnitude of the contribution of this interaction to the free energy. As mentioned above, there is no satisfactory description of ions with bound states, He^+ in the present context, immersed in a surrounding dense plasma. Indeed, it is difficult to capture the drastically different nature of the short- and long-range interactions of such species with surrounding charged particles. This is undoubtedly a limitation of the chemical picture, and of the related distinction between different entities. In reality, the concept of identifying He^+ or He^{2+} particles, based on the concept of a potential or pseudopotential, becomes meaningless at high density. Only at high temperature, when kinetic contributions dominate, is the approach conceptually correct. Therefore, although He^+ and He^{2+} are distinguishable in our model free energy, we do not pretend to give an accurate description of the second stage of helium pressure ionization, from He^+ to He^{2+}. As detailed in the next section, however, we have checked that the present, crude description of the He^+-He^{2+} interactions does not alter the final phase diagram. The reason is that, at least in the present model, helium pressure ionization proceeds directly from atomic helium He to fully ionized helium He^{2+}, or at least to a strongly ionized stage. It will certainly be interesting to compare these results with experiments and with results obtained with first-principles calculations, although these latter will certainly have to face their own difficulties in this complex regime.

4. Summary

Summarizing the various contributions described in the previous sections, and following Eqs. (4) and (9), the full model free energy reads

$$\begin{aligned}\frac{\beta F}{N_{\rm tot}}(V,T,\{N_i\}) = &-\sum_{i={\rm He,He^+}}\frac{N_i}{N_{\rm tot}}\left\{1+\ln\left[\frac{V}{N_i}\left(\frac{2\pi Mk_BT}{h^2}\right)^{3/2}\right]\right\} - \sum_{i={\rm He,He^+}}\frac{N_i}{N_{\rm tot}}\ln\sum_\alpha g_{i\alpha}\omega_{i\alpha}^{\rm HS}\omega_{i\alpha}^{\mu E}e^{-\beta E_{i\alpha}}\\ &+\frac{\beta F_{\rm HS}(\{N_{{\rm He},\alpha},N_{\rm He^+,\alpha},N_{\rm He^{2+}}\},\{\sigma_{{\rm He},\alpha},\sigma_{\rm He^+,\alpha},\sigma_{\rm He^{2+}}=0\},V,T)}{N_{\rm tot}}\\ &-\sum_{i=\{{\rm He},\alpha\},\{{\rm He^+},\alpha\}}\frac{N_i}{N_{\rm tot}}\frac{\beta\partial F_{\rm HS}(\{N_i\},\{\sigma_{{\rm He},\alpha},\sigma_{\rm He^+,\alpha}\},V,T)}{\partial N_i}+\frac{\beta F_{\rm pol}({\rm He,He^+,He^{2+}},N_{e^-},V,T)}{N_{\rm tot}}\end{aligned}$$

$$+\frac{\beta N_{\rm tot}}{2V}\sum_{i,j={\rm He,He^+}}\frac{N_i}{N_{\rm tot}}\frac{N_j}{N_{\rm tot}}\int d\boldsymbol{r}\,\Phi^{ij}_{\rm pert}(r)e^{-\beta\Phi^{ij}_{\rm ref}(r)}y^{ij}_{\rm HS}(r)$$

$$+\frac{\hbar^2}{24(k_BT)^2M_{\rm He}}\frac{N_{\rm tot}}{V}\sum_{i,j={\rm He,He^+}}\frac{N_i}{N_{\rm tot}}\frac{N_j}{N_{\rm tot}}\int d\boldsymbol{r}\,\boldsymbol{\nabla}^2\Phi(r)e^{-\beta\Phi^{ij}(r)}y^{ij}_{\rm HS}(r)+\frac{N_{\rm He^+}N_{\rm He^{2+}}}{2N_{\rm tot}^2}Z_1Z_2\frac{e^2}{a}-\frac{3}{2}\frac{N_{\rm He^+}}{N_{\rm tot}}\frac{(Z_1e)^2}{a}$$

$$+\frac{\beta F^{\rm FIP}(V,T,N_{\rm He^{2+}},N_{e^-})}{N_{\rm tot}},\qquad(20)$$

where $N_{\rm tot}=N_{\rm He}+N_{\rm He^+}+N_{\rm He^{2+}}$. Note that $\omega^{\rm HS}_{i\alpha}\omega^{\mu E}_{i\alpha}$ include the occupation probabilities calculated from interactions with neutral surrounding particles [hard-sphere interaction, Eq. (11)] and with charged surrounding particles [microfield interaction, Eq. (18)].

The equilibrium populations are derived from the minimization of the free energy $F(V,T,\{N_i\})$ with respect to two independent variables, given the conditions of mass conservation $N_{\rm He^{2+}}=N_{\rm tot}-N_{\rm He^+}-N_{\rm He}$ and electroneutrality $N_{e^-}=N_{\rm He^+}+2N_{\rm He^{2+}}$:

$$\left.\frac{\partial(\beta F/N_{\rm tot})}{\partial N_{\rm He}}\right|_{T,V,N_{\rm He^+}}=0=\left.\frac{\partial(\beta F/N_{\rm tot})}{\partial N_{\rm He^+}}\right|_{T,V,N_{\rm He}}.\qquad(21)$$

Convergence of this two-dimensional minimization is achieved when the change in the populations from one iteration to the next one is less than one part in 3×10^{-7}. The various thermodynamic quantities are then calculated from appropriate derivations of the free energy.

IV. RESULTS

As mentioned previously, our free-energy model, with the He-He potential calibrated on sound velocity measurements [17], reproduces the available Hugoniot experiments [18] (see Fig. 4). We have also checked that we recover the results of the Saha equations in the low-density limit and, by construction, the fully ionized plasma model at high density. An example is shown in Fig. 5 for $T=10^{4.7}$ K. The vanishing fraction of bound species populations for $\rho\gtrsim10$ g cm^{-3} illustrates the onset of pressure ionization.

We have also checked that we recover the results of Aparicio and Chabrier [1] for pure atomic helium in the low-density, low-temperature regime until pressure ionization sets in (see Fig. 6 for $T=10^{3.5}$ K).

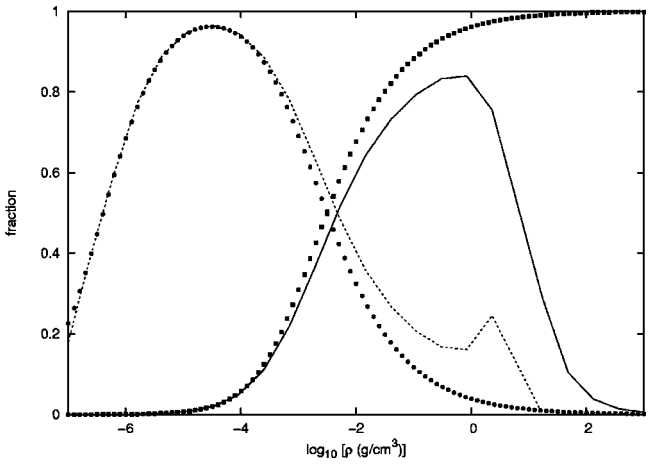

FIG. 5. Comparison between the populations obtained with our model (lines) and those corresponding to the Saha equations (symbols). The solid (dotted) line corresponds to the He (He^+) fraction. The temperature is $T=10^{4.7}$ K.

A. Limitations of the model

As mentioned earlier, our free-energy minimization method is rooted in the chemical approach. It is based on a heuristic treatment of the dominant physical effects responsible for the thermodynamic properties of dense atomic or ionized helium. Although it certainly retains some degree of reality, this model cannot pretend to give an exact description of these properties, and the results should depend to some extent on the main approximations used in the model. We examine this issue in the present section.

1. Lower boundary for σ_1

At very high density, the WCA radii tend eventually to zero, as shown in Fig. 1. This favors the He and He^+ species

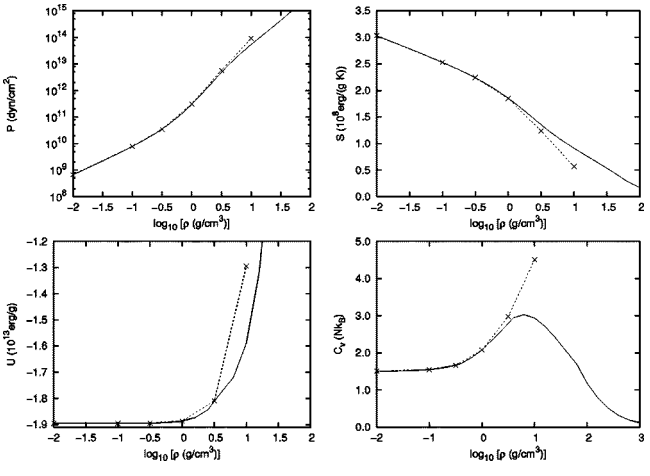

FIG. 6. Comparison between the present model (solid lines) and the results of Aparicio and Chabrier [1] (dotted lines with symbols), which do not include pressure ionization, for the pressure, the massic entropy, the massic internal energy, and the specific heat at $T=10^{3.5}$ K.

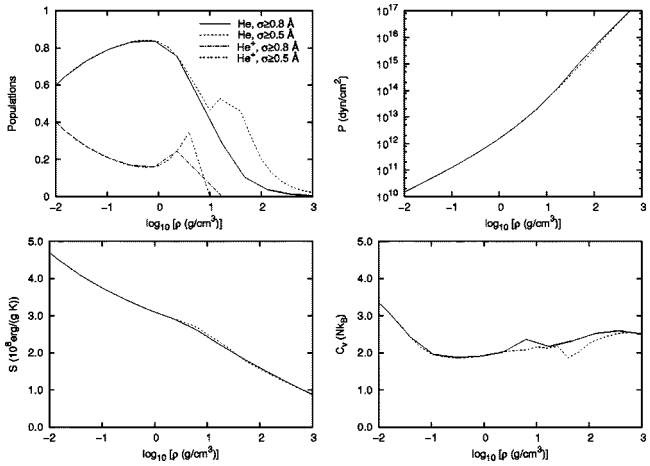

FIG. 7. Effect of the lower boundary for σ_1 on the populations, the pressure, the massic entropy, and the specific heat as a function of the density. The solid lines correspond to the case $\sigma_1 \geqslant 0.8$ Å, the dotted lines to the case $\sigma_1 \geqslant 0.5$ Å; the temperature is $T=10^{4.7}$ K.

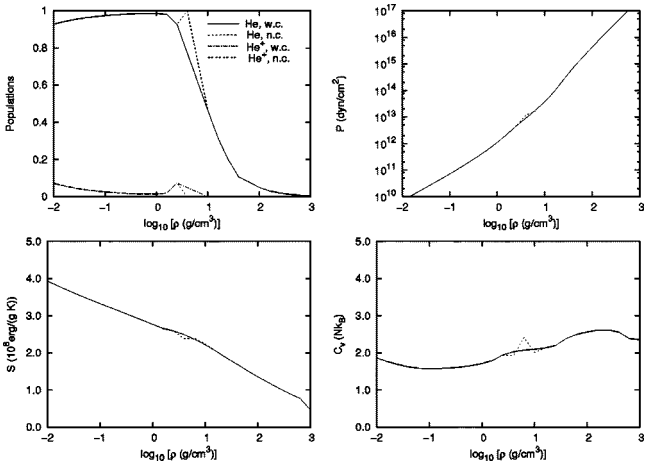

FIG. 8. Effect of the description of the He^+-He^{2+} and He^+-e^- couplings on the populations (w.c. $\equiv$ with coupling, n.c. $\equiv$ no coupling), the pressure, the massic entropy, and the specific heat as a function of the density. If not specified, the solid line corresponds to the case with coupling and the dotted line to the case without any coupling; the temperature is $T=10^{4.5}$ K.

and thus prevent pressure ionization to occur, a well identified artifact of the chemical picture [4,30]. In order to prevent such an unphysical behavior, we define arbitrarily a lower limit for σ_{He} and σ_{He^+}. Figure 7 (for the $10^{4.7}$ K isotherm) illustrates the effect of this approximation for $\sigma_1 \geqslant 0.8$ Å and $\sigma_1 \geqslant 0.5$ Å.

Not surprisingly, the choice of a lower limit for σ_1 affects appreciably the populations in the very regime of pressure ionization. However, the effect is almost inconsequential on the thermodynamic quantities, the very purpose of the present calculations. This stems from the fact that the bound species do not contribute to the free energy when they are associated with a very small radius. The final model calculations were made with $\sigma_1=0.8$ Å.

2. Polarizability of He-He$^+$

We have also tested the influence of the polarizability α_i which appears in the He-He^+ potential, and which has been taken equal to the volume $\sigma^3_{\mathrm{He\text{-}He^+}}$. Calculations conducted with a value of α_i reduced or increased by a factor of 10 left the results nearly unaffected. This can be easily understood as in the domain where nonideal effects play a role, He and He^+ do not coexist in comparable fractions most of the time. Moreover, the contribution of F_{pol} to the total free energy remains always marginal.

3. Validity of the quantum correction F_{qm}

As mentioned in Sec. III A 4, we have used the first-order term of the Wigner-Kirkwood expansion to take into account the quantum effects between atomic centers. This expansion becomes invalid at high density and low temperature. As a rule of thumb, the domain of reliability of the expansion is given by $\log_{10}[T\ (\mathrm{K})]-\log_{10}[\rho\ (\mathrm{g/cm^3})] \gtrsim 2$. Such a limitation has no consequence in an astrophysical context, as no astrophysical object with a helium composition exists beyond this limit.

4. Influence of the He^+-He^{2+} coupling

As mentioned in Sec. III D 3, the long-range interaction between He^+, He^{2+}, and e^- is treated in a rather crude way in the present model. We have tested the influence of this approximation by submitting a few tests without this term. The results are illustrated in Fig. 8 for $T=10^{4.5}$ K. We have checked other isotherms, and the conclusion is that the EOS and its derivatives are nearly independent of this coupling term except in a very limited temperature-density range. As illustrated in the next section, but also on Figs. 5, 7, and 8, the reason is that pressure ionization occurs directly from He to He^{2+}, with no regions where He^+ and He^{2+} coexist in comparable number, except at high temperature ($T \gtrsim 10^5$ K) where temperature ionization dominates. Although we certainly cannot rule out the fact that this is an artifact of our model, a possible physical explanation might be the large differences between the ground-state energies of the different species, much larger than for hydrogen. The contribution of the ground-state energy of He to the total free energy thus prevents partial ionization from occurring, favoring the atomic phase. As mentioned previously, it will be interesting to compare this prediction with experimental results and first-principles calculations, once they become available, to verify whether this behavior is a flaw of the present model or whether it reflects the behavior of helium pressure ionization, an extremely interesting issue.

B. Thermodynamical quantities

A subset of our final EOS calculations, based on the model free energy (20) is presented in Tables I–III, corresponding to Fig. 9 (for the pressure), Fig. 10 (for the massic entropy), and Fig. 11 (for the specific heat). For these calculations, ten internal levels have been considered, for both He and He^+. These ten levels are enough to represent the internal partition function as the highest levels are always destroyed

TABLE I. Equation of state for the isotherm $T=10^{3.8}$ K. For each value of the density are given the abundances of He, He^+, and He^{2+}, the pressure, the massic entropy, the massic internal energy (with a zero of energy corresponding to the fully ionized plasma at zero temperature), and the specific heat.

$\log_{10}[\rho\ (g/cm^3)]$	x_{He}	x_{He^+}	$x_{He^{2+}}$	P (dyn/cm^2)	S (erg/g/K)	U (erg/g)	$C_v(Nk_B)$
−2.00	1.0000×10^{0}	0.0000×10^{0}	0.0000×10^{0}	0.1330×10^{10}	0.3246×10^{9}	-0.1886×10^{14}	0.1504×10^{1}
−1.60	1.0000×10^{0}	0.0000×10^{0}	0.0000×10^{0}	0.3409×10^{10}	0.3052×10^{9}	-0.1886×10^{14}	0.1510×10^{1}
−1.20	1.0000×10^{0}	0.0000×10^{0}	0.0000×10^{0}	0.9003×10^{10}	0.2854×10^{9}	-0.1886×10^{14}	0.1527×10^{1}
−0.80	1.0000×10^{0}	0.0000×10^{0}	0.0000×10^{0}	0.2554×10^{11}	0.2646×10^{9}	-0.1885×10^{14}	0.1565×10^{1}
−0.40	1.0000×10^{0}	0.0000×10^{0}	0.0000×10^{0}	0.8538×10^{11}	0.2415×10^{9}	-0.1883×10^{14}	0.1670×10^{1}
0.00	1.0000×10^{0}	0.0000×10^{0}	0.0000×10^{0}	0.4092×10^{12}	0.2141×10^{9}	-0.1873×10^{14}	0.1929×10^{1}
0.40	1.0000×10^{0}	0.0000×10^{0}	0.0000×10^{0}	0.3037×10^{13}	0.1816×10^{9}	-0.1828×10^{14}	0.2301×10^{1}
0.60	1.0000×10^{0}	0.0000×10^{0}	0.0000×10^{0}	0.8729×10^{13}	0.1646×10^{9}	-0.1762×10^{14}	0.2513×10^{1}
0.80	0.7158×10^{0}	0.1688×10^{-4}	0.2842×10^{0}	0.1082×10^{14}	0.1484×10^{9}	-0.1632×10^{14}	0.2693×10^{1}
1.00	0.4316×10^{0}	0.2531×10^{-4}	0.5684×10^{0}	0.2210×10^{14}	0.1324×10^{9}	-0.1502×10^{14}	0.2822×10^{1}
1.20	0.3144×10^{0}	0.2531×10^{-4}	0.6856×10^{0}	0.7143×10^{14}	0.1161×10^{9}	-0.1307×10^{14}	0.2878×10^{1}
1.40	0.1983×10^{0}	0.2531×10^{-4}	0.8017×10^{0}	0.2314×10^{15}	0.9875×10^{8}	-0.8728×10^{13}	0.2841×10^{1}
1.60	0.1062×10^{0}	0.1688×10^{-4}	0.8938×10^{0}	0.6832×10^{15}	0.7975×10^{8}	-0.5620×10^{12}	0.2689×10^{1}
2.00	0.4980×10^{-1}	0.1688×10^{-4}	0.9502×10^{0}	0.4249×10^{16}	0.4101×10^{8}	0.2846×10^{14}	0.2098×10^{1}
2.40	0.1980×10^{-1}	0.1688×10^{-4}	0.9802×10^{0}	0.2338×10^{17}	0.1681×10^{8}	0.9215×10^{14}	0.1360×10^{1}
2.80	0.7880×10^{-2}	0.1125×10^{-4}	0.9921×10^{0}	0.1197×10^{18}	0.4317×10^{7}	0.2210×10^{15}	0.6508×10^{0}

even for the lowest density we are considering. No He doubly excited states have been considered in our calculation. This is a reasonable approximation for the two following reasons. First of all, the high energy cost of these states (the first doubly excited state lies ~60 eV above the He ground state) disfavors their formation (in a way similar to the direct ionization of He to He^{2+} without any He^+ state; see the following discussion). The second reason is their rapid decay by autoionization (typically in 10^{-13}–10^{-14} s). It is therefore unlikely that these states survive in the midst of interacting neighbor particles. The zero of energy corresponds to the fully ionized plasma at zero temperature. The rising behavior of C_V for $\log_{10}[\rho\ (g/cm^3)] \gtrsim -1$ stems from correlations between helium atoms (configurational free energy), since all excited levels are destroyed at this density, at least for the coolest temperature. The drop at larger density reflects pressure ionization, from He to He^{2+}. We also present in Fig. 12 the phase diagram of helium. The lines separate the different

TABLE II. Equation of state for the isotherm $T=10^{4.2}$ K. For each value of the density are given the abundances of He, He^+, and He^{2+}, the pressure, the massic entropy, the massic internal energy (with a zero of energy corresponding to the fully ionized plasma at zero temperature), and the specific heat.

$\log_{10}[\rho\ (g/cm^3)]$	x_{He}	x_{He^+}	$x_{He^{2+}}$	P (dyn/cm^2)	S (erg/g/K)	U (erg/g)	$C_v(Nk_B)$
−2.00	0.9995×10^{0}	0.4950×10^{-3}	0.0000×10^{0}	0.3327×10^{10}	0.3536×10^{9}	-0.1856×10^{14}	0.1505×10^{1}
−1.60	0.9997×10^{0}	0.3000×10^{-3}	0.0000×10^{0}	0.8474×10^{10}	0.3342×10^{9}	-0.1856×10^{14}	0.1508×10^{1}
−1.20	0.9998×10^{0}	0.1800×10^{-3}	0.0000×10^{0}	0.2203×10^{11}	0.3146×10^{9}	-0.1856×10^{14}	0.1519×10^{1}
−0.80	0.9999×10^{0}	0.1100×10^{-3}	0.0000×10^{0}	0.6004×10^{11}	0.2944×10^{9}	-0.1854×10^{14}	0.1549×10^{1}
−0.40	0.9999×10^{0}	0.6750×10^{-4}	0.0000×10^{0}	0.1817×10^{12}	0.2730×10^{9}	-0.1850×10^{14}	0.1618×10^{1}
0.00	0.9999×10^{0}	0.6000×10^{-4}	0.0000×10^{0}	0.6898×10^{12}	0.2493×10^{9}	-0.1837×10^{14}	0.1765×10^{1}
0.40	1.0000×10^{0}	0.0000×10^{0}	0.0000×10^{0}	0.3814×10^{13}	0.2228×10^{9}	-0.1785×10^{14}	0.1996×10^{1}
0.60	1.0000×10^{0}	0.0000×10^{0}	0.0000×10^{0}	0.9964×10^{13}	0.2091×10^{9}	-0.1717×10^{14}	0.2142×10^{1}
0.80	0.7325×10^{0}	0.1688×10^{-4}	0.2675×10^{0}	0.1295×10^{14}	0.2043×10^{9}	-0.1593×10^{14}	0.2336×10^{1}
1.00	0.4650×10^{0}	0.2531×10^{-4}	0.5350×10^{0}	0.2660×10^{14}	0.1923×10^{9}	-0.1469×10^{14}	0.2442×10^{1}
1.20	0.2405×10^{0}	0.2531×10^{-4}	0.7595×10^{0}	0.7335×10^{14}	0.1751×10^{9}	-0.1257×10^{14}	0.2489×10^{1}
1.40	0.1983×10^{0}	0.2531×10^{-4}	0.8017×10^{0}	0.2305×10^{15}	0.1551×10^{9}	-0.8125×10^{13}	0.2507×10^{1}
1.60	0.1062×10^{0}	0.1688×10^{-4}	0.8938×10^{0}	0.7012×10^{15}	0.1345×10^{9}	0.1229×10^{12}	0.2526×10^{1}
2.00	0.4980×10^{-1}	0.1688×10^{-4}	0.9502×10^{0}	0.4294×10^{16}	0.9833×10^{8}	0.2923×10^{14}	0.2573×10^{1}
2.40	0.1980×10^{-1}	0.1688×10^{-4}	0.9802×10^{0}	0.2346×10^{17}	0.5425×10^{8}	0.9255×10^{14}	0.2456×10^{1}
2.80	0.7880×10^{-2}	0.1125×10^{-4}	0.9921×10^{0}	0.1199×10^{18}	0.2836×10^{8}	0.2213×10^{15}	0.1865×10^{1}

TABLE III. Equation of state for the isotherm $T=10^{4.5}$ K. For each value of the density are given the abundances of He, He^+, and He^{2+}, the pressure, the massic entropy, the massic internal energy (with a zero of energy corresponding to the fully ionized plasma at zero temperature), and the specific heat.

$\log_{10}[\rho\ (g/cm^3)]$	x_{He}	x_{He^+}	$x_{He^{2+}}$	P (dyn/cm^2)	S (erg/g/K)	U (erg/g)	$C_v(Nk_B)$
−2.00	0.9287×10^{0}	0.7128×10^{-1}	0.0000×10^{0}	0.7083×10^{10}	0.3936×10^{9}	-0.1758×10^{14}	0.1862×10^{1}
−1.60	0.9532×10^{0}	0.4680×10^{-1}	0.0000×10^{0}	0.1757×10^{11}	0.3676×10^{9}	-0.1775×10^{14}	0.1689×10^{1}
−1.20	0.9690×10^{0}	0.3102×10^{-1}	0.0000×10^{0}	0.4441×10^{11}	0.3439×10^{9}	-0.1786×10^{14}	0.1590×10^{1}
−0.80	0.9788×10^{0}	0.2124×10^{-1}	0.0000×10^{0}	0.1169×10^{12}	0.3216×10^{9}	-0.1790×10^{14}	0.1582×10^{1}
−0.40	0.9848×10^{0}	0.1524×10^{-1}	0.0000×10^{0}	0.3322×10^{12}	0.2995×10^{9}	-0.1789×10^{14}	0.1619×10^{1}
0.00	0.9862×10^{0}	0.1376×10^{-1}	0.0000×10^{0}	0.1098×10^{13}	0.2769×10^{9}	-0.1773×10^{14}	0.1715×10^{1}
0.40	0.9271×10^{0}	0.7296×10^{-1}	0.0000×10^{0}	0.4567×10^{13}	0.2590×10^{9}	-0.1699×10^{14}	0.1947×10^{1}
0.60	0.8063×10^{0}	0.7988×10^{-1}	0.1139×10^{0}	0.9005×10^{13}	0.2492×10^{9}	-0.1651×10^{14}	0.2031×10^{1}
0.80	0.6457×10^{0}	0.5800×10^{-1}	0.2964×10^{0}	0.1788×10^{14}	0.2366×10^{9}	-0.1527×10^{14}	0.2073×10^{1}
1.00	0.4726×10^{0}	0.2536×10^{-1}	0.5020×10^{0}	0.3791×10^{14}	0.2218×10^{9}	-0.1403×10^{14}	0.2099×10^{1}
1.20	0.3144×10^{0}	0.2531×10^{-4}	0.6856×10^{0}	0.9098×10^{14}	0.2050×10^{9}	-0.1189×10^{14}	0.2132×10^{1}
1.40	0.1983×10^{0}	0.2531×10^{-4}	0.8017×10^{0}	0.2619×10^{15}	0.1867×10^{9}	-0.7390×10^{13}	0.2198×10^{1}
1.60	0.1062×10^{0}	0.1688×10^{-4}	0.8938×10^{0}	0.7280×10^{15}	0.1700×10^{9}	0.9305×10^{12}	0.2387×10^{1}
2.00	0.4980×10^{-1}	0.1688×10^{-4}	0.9502×10^{0}	0.4359×10^{16}	0.1356×10^{9}	0.3008×10^{14}	0.2563×10^{1}
2.40	0.1980×10^{-1}	0.1688×10^{-4}	0.9802×10^{0}	0.2364×10^{17}	0.1049×10^{9}	0.9382×10^{14}	0.2619×10^{1}
2.80	0.7880×10^{-2}	0.1125×10^{-4}	0.9921×10^{0}	0.1203×10^{18}	0.7731×10^{8}	0.2226×10^{15}	0.2386×10^{1}

domains where either He, He^+, or He^{2+} is the dominant species, i.e., represents a fraction larger than 50%. As mentioned previously, an interesting prediction of this diagram (see also the tables) is that for $T\lesssim10^5$ K, pressure ionization, defined as $x_{He^{2+}}\gtrsim0.5$, proceeds directly from He to He^{2+} at $\rho\gtrsim10$ g cm^{-3}, i.e., $P\gtrsim20$ Mbar. As mentioned in Sec. IV A 4, the sharp transition due to pressure ionization, from $x_{He}\gtrsim0.5$ to $x_{He^{2+}}\gtrsim0.5$ at $\rho\sim10$ g cm^{-3} (see tables), and the persistence of atomic helium at high density, might reflect the large energy cost of the ground-state energies of ionized species (24.587 and 79.003 eV) to the total free energy. Eventually, abrupt ionization occurs from He to He^{2+}, unless temperature is high enough to unbound one of the two electrons from the helium atom. This is corroborated by the fact that the pressure ionization of He^+ (which happens if $T\gtrsim10^5$ K) occurs at lower densities $\rho\gtrsim1$ g cm^{-3}. This phase diagram can be compared with the one for hydrogen [31]. For deuterium, the EOS is essentially the same as for hydrogen providing the nucleus mass is rescaled [5]. However, for helium, because of the $Z=2$ nucleus and the induced electronic structures, the phase diagram is different, and pressure ionization occurs at larger pressures than for H or D.

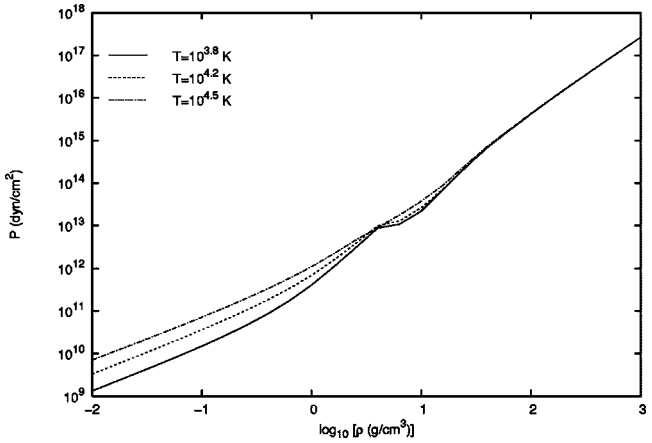

FIG. 9. Pressure as a function of the density for three isotherms. Solid line, $T=10^{3.8}$ K; dotted line, $T=10^{4.2}$ K; dot-dashed line, $T=10^{4.5}$ K.

V. CONCLUSION

In this paper, we have computed a free-energy model aimed at deriving the thermodynamic quantities of dense fluid helium, from the low-density atomic domain to the high-density fully ionized regime, covering the regime of partial ionization. The model is based on the so-called chemical picture for the description of the interactions be-

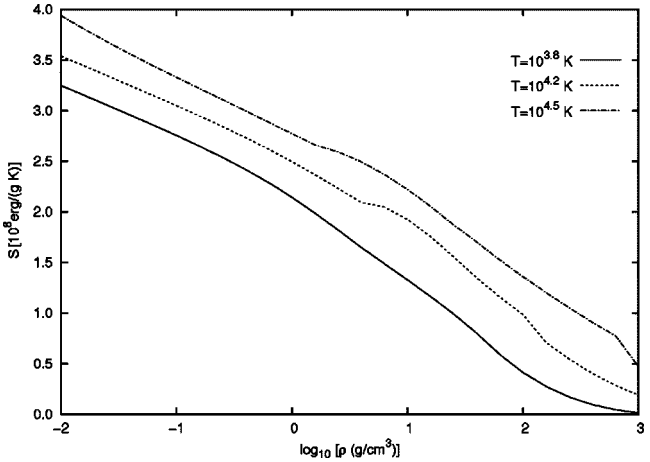

FIG. 10. Same as Fig. 9 for the massic entropy.

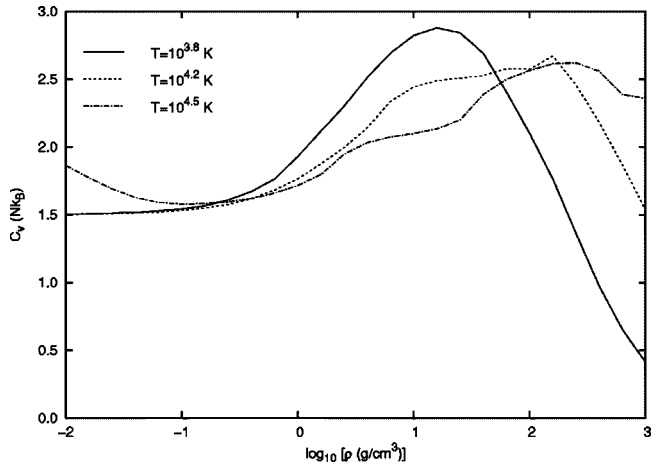

FIG. 11. Same as Fig. 9 for the specific heat.

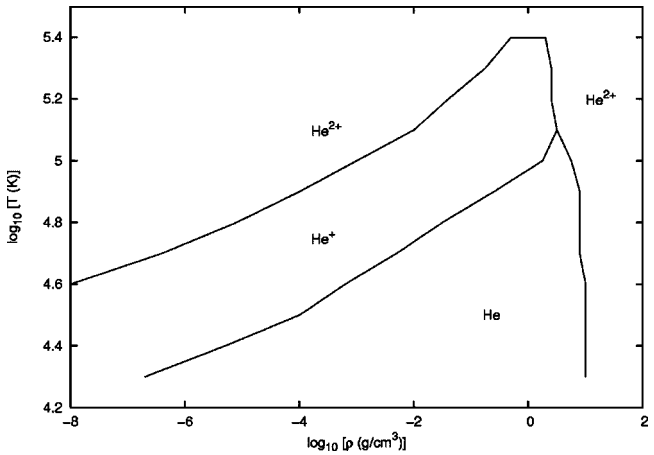

FIG. 12. Phase diagram of helium. The lines separate the different domains of predominance of the different species He, He^+, and He^{2+}.

tween the different species in the fluid. The abundances of the various atomic and ionic components are obtained through minimization of the free energy. Despite the shortcomings inherent to the chemical approach, we believe the present model to give a reasonable description of the equation of state of dense helium, including the regime of pressure ionization. Although the basis of the model becomes of doubtful validity in this latter domain, this affects only limited regions of the temperature-density diagram. Comparisons with available sound speed measurements and shock-wave experiments for atomic helium assess the validity of the model up to the megabar range, whereas at very high density the model recovers the fully ionized plasma model and thus Monte Carlo simulations of the thermodynamic properties of the so-called one-component plasma (OCP) model. Although the present model cannot pretend giving a precise determination of the various atomic and ionic concentrations in the fluid, at least in the pressure ionization regimes, it yields a reasonably accurate determination of the phase diagram of dense, fluid helium with its various $He/He^+/He^{2+}$ ionization contours. For $T \lesssim 10^5$ K, pressure ionization is found to occur directly from atomic helium He to fully ionized helium He^{2+}, or at least to a strongly ionized state, without the He^+ stage ($x_{He^+} <$ a few percent). It would be interesting to test such a prediction with high-pressure dynamical experiments. Indeed, such a behavior of the phase diagram bears important consequences for the thermodynamic, magnetic, and transport properties of the interior of cool and dense astrophysical objects, including giant planets. In all cases, *pressure* ionization is found to occur around $\rho \sim 10$ g cm^{-3}, i.e., $P \sim 20 \times 10^6$ bar. Detailed explorations of the sensitivity of the results to various approximations entering the free-energy model show that they remain inconsequential for the first derivatives of the free energy over most of the phase diagram. In some limited regions, however, characteristic of the pressure ionization regime, maximum variations of the entropy and the pressure can reach $\sim 5\%$ and $\sim 20\%$, respectively, in the worst case. Although still modest in most cases, the uncertainties become larger for second derivatives, in particular the ones directly related to the different degrees of freedom and thus to the relative populations, like the specific heat. As mentioned above, however, only limited regions of the phase diagram are concerned by the regime where various species coexist in comparable numbers. As a whole, the present model remains simple enough to allow the calculation of the EOS of dense helium over an extended domain of pressure and density, a necessary condition for applications to the computation of stellar and giant planet internal structure and high-pressure experiment diagnostics.

Besides its astrophysical interest, the calculation of the phase diagram of dense helium is of intrinsic theoretical interest. Indeed, comparison betwen these calculations and near-future high-pressure shock-wave or laser experiments will allow a better determination of the domains of validity of the present model and of the possible improvements. By such, these comparisons will yield a better understanding of the properties of matter under extreme conditions, and more specifically of the complex regime of matter pressure ionization and metallization.

ACKNOWLEDGMENTS

We are very grateful to Alexander Potekhin and Gérard Massacrier for very useful discussions and insightful remarks.

[1] J. Aparicio and G. Chabrier, Phys. Rev. E **50**, 4948 (1994).
[2] G. Chabrier and A. Potekhin, Phys. Rev. E **58**, 4941 (1998).
[3] A. Potekhin and G. Chabrier, Phys. Rev. E **62**, 8554 (2000).
[4] D. Saumon and G. Chabrier, Phys. Rev. A **46**, 2084 (1992).
[5] D. Saumon, G. Chabrier, D. Wagner, and X. Xie, High Press. Res. **16**, 331 (2000).
[6] H. Graboske, D. J. Harwood, and F. J. Rogers, Phys. Rev. **186**, 210 (1969).
[7] G. Fontaine, H. Graboske, and H. van Horn, Astrophys. J., Suppl. **35**, 293 (1977).
[8] L. Landau and E. Lifchitz, *Statistical Physics*, 3rd ed., Course of Theoretical Physics Vol. 5 (Pergamon, Oxford, 1980), Part 1.
[9] J. Weeks, D. Chandler, and H. Andersen, J. Chem. Phys. **54**, 5237 (1971).
[10] J. Weeks, D. Chandler, and H. Andersen, J. Chem. Phys. **55**, 5422 (1971).
[11] H. Kang, C. Lee, T. Ree, and F. Ree, J. Chem. Phys. **82**, 414 (1985).
[12] L. Verlet and J. Weis, Phys. Rev. A **5**, 939 (1972).
[13] G. Mansoori, N. Carnahan, K. Starling, and T. Leland, Jr., J. Chem. Phys. **54**, 1523 (1971).
[14] E. Grundke and D. Henderson, Mol. Phys. **24**, 269 (1972).
[15] R. Aziz and M. Slaman, J. Chem. Phys. **94**, 8047 (1991).
[16] D. Ceperley and H. Partridge, J. Chem. Phys. **84**, 820 (1986).
[17] R. Le Toullec, P. Loubeyre, and J. Pinceaux, Phys. Rev. B **40**, 2368 (1989).
[18] W. Nellis, A. Holmes, R. Trainor, G. Governo, M. Ross, and D. Young, Phys. Rev. Lett. **53**, 1248 (1984).
[19] D. Hummer and D. Mihalas, Astrophys. J. **331**, 794 (1988).
[20] D. Saumon and G. Chabrier, Phys. Rev. A **44**, 5122 (1991).
[21] W. Wiese, D. Kelleher, and D. Paquette, Phys. Rev. A **6**, 1132 (1972).
[22] B. Grabowski, J. Halenka, and J. Madej, Astrophys. J. **313**, 750 (1987).
[23] J. Seidel, S. Arndt, and W. Kraeft, Phys. Rev. E **52**, 5387 (1995).
[24] E. Wigner, Phys. Rev. **40**, 749 (1932).
[25] J. Kirkwood, Phys. Rev. **44**, 31 (1933).
[26] G. Chabrier, J. Phys. (Paris) **51**, 1607 (1990).
[27] W. Ebeling, A. Förster, W. Richert, and H. Hess, Physica A **150**, 159 (1988).
[28] A. Potekhin, G. Chabrier, and D. Gilles, Phys. Rev. E **65**, 036412 (2002).
[29] E. Salpeter, Astrophys. J. **134**, 669 (1961).
[30] A. Potekhin, Phys. Plasmas **3**, 4156 (1996).
[31] D. Saumon, G. Chabrier, and H. M. van Horn, Astrophys. J., Suppl. Ser. **99**, 713 (1995).